

Article

Investigation of the Oxidation Mechanism of Dopamine Functionalization in an AZ31 Magnesium Alloy for Biomedical Applications

Arezoo Ghanbari ¹, Fernando Warchomicka ^{2,*}, Christof Sommitsch ²  and Ali Zamanian ^{1,*} 

¹ Department of Nano-Technology and Advanced Materials, Institute of Materials and Energy (MERC), 31787-316 Alborz, Iran; ghanbariarezo091@gmail.com

² Institute of Materials Science, Joining and Forming, Graz University of Technology, Kopernikusgasse 24/I, A-8010 Graz, Austria; christof.sommitsch@tugraz.at

* Correspondence: fernando.warchomicka@tugraz.at (F.W.); a-zamanian@merc.ac.ir (A.Z.); Tel.: +43-316-873-1654 (F.W.); +98-912-321-1180 (A.Z.)

Received: 9 July 2019; Accepted: 12 September 2019; Published: 16 September 2019



Abstract: Implant design and functionalization are under significant investigation for their ability to enhance bone-implant grafting and, thus, to provide mechanical stability for the device during the healing process. In this area, biomimetic functionalizing polymers like dopamine have been proven to be able to improve the biocompatibility of the material. In this work, the dip coating of dopamine on the surface of the magnesium alloy AZ31 is investigated to determine the effects of oxygen on the functionalization of the material. Two different conditions are applied during the dip coating process: (1) The absence of oxygen in the solution and (2) continuous oxygenation of the solution. Energy dispersive spectroscopy (EDS) and Fourier transform infrared spectroscopy (FTIR) are used to analyze the composition of the formed layers, and the deposition rate on the substrate is determined by molecular dynamic simulation. Electrochemical analysis and cell cultivation are performed to determine the corrosion resistance and cell's behavior, respectively. The high oxygen concentration in the dopamine solution promotes a homogeneous and smooth coating with a drastic increase of the deposition rate. Also, the addition of oxygen into the dip coating process increases the corrosion resistance of the material.

Keywords: biodegradable magnesium; dopamine; Impedance behavior; molecular dynamic simulation

1. Introduction

Magnesium implants have intrigued the medical industry as a way to substitute temporary implants with more permanent counterparts. In the application of temporary fasteners, including screws or pins, magnesium implants are superior to permanent titanium or stainless-steel implants, since their use eliminates the need for second surgery to remove the implant after bone healing. Moreover, magnesium alloys provide mechanical properties with close compatibility with bone, thereby decreasing the risk of stress shielding [1,2]. As with other bio metals, magnesium is investigated to promote the cell's response on the surface. The healing rate of bone is critical [3], and, for successful bone regeneration, cell viability is highly significant [4]. Cell adhesion is unlikely to occur directly on the implant. Thus, an appropriate surface treatment is needed [5]. For this treatment, several biomimetic coatings are investigated: Aminopropyltriethoxysilane, vitamin C (AV), carbonyldiimidazole (CDI), stearic acid (SA), aminated hydroxyethyl cellulose, gelatin, and peptides [5–9]. Depending on the composition, biomimetic coatings can have the capability to retard the corrosion affinity of magnesium to body fluids [5,8,9]. Therefore, a biomimetic coating should be adhesive and compact enough to

protect the substrate against corrosive body fluid. In this area of study, polydopamine is introduced as a biomimetic coating to enhance the adhesion of other biomimetic coatings [10]. For instance, the use of a coating made by gelatin (a mixture of peptides and proteins) and modified with polydopamine can improve the binding affinity between the coating and the metal (e.g., on a titanium surface [11]) or promote corrosion resistance [12]. In other cases, the use of dopamine helps to immobilize functional molecules as a robust anchor in biofunctional surfaces (e.g., nano magnetic particles [13]) or increase the cytocompatibility and osteogenic potential of the scaffold [14], among other examples.

Recent works on magnesium have shown the advantage of using a functionalized surface with dopamine to enhance corrosion resistance [15–17], as well as the cell proliferation on the surface of the implant [17,18]. Inspired by the composition of adhesive proteins in mussels, dopamine can be self-polymerized to form a surface-adherent, thin, and robust film on almost all kinds of materials, including organic and inorganic ones [19]. In this area, the dip coating method [15–17,20] has been used as a convenient way to anchor the dopamine and create a film on magnesium alloys. In situ spontaneous deposition takes place through an aerobic auto-oxidation mechanism in a mildly basic aqueous buffered media and, consequently, a bio-inspired film is generated on the substrate. Although the film is known as polydopamine, there is controversy over whether the film consists of supramolecular or monomer aggregates or has a polymeric structure [21]. The oxidation mechanism during the dopamine coating and the evolution of the molecules have been deeply investigated [18,20,22–25]. Many oxidants were evaluated as a buffer for the formation of the coating, including compounds like copper sulfate, sodium periodate, and ammonium peroxydisulfate [25,26], and oxygen as a biocompatible oxidant [20,23,25,26]. It is reported that polydopamine or dopamine-melanin film deposition seems to depend not only on the monomer's availability but also on the availability of O₂ [16,25].

Whether polydopamine is incorporated in a magnesium implant as an adhesive intermediate biomimetic layer or an individual biomimetic layer, the corrosion rate of this layer is fundamental. The present work focuses the investigation on variation of the corrosion resistance of the AZ31 alloy through functionalization of the surface via dopamine, with the presence and absence of oxygen. Oxygen is selected as a condition variable to investigate the effects of an oxidant on the coating's quality.

2. Materials and Methods

2.1. Substrate

The magnesium alloy AZ31 was used in this work. The chemical composition of AZ31, in wt.%, is as follows: 3 Al, 0.4 Mn, 0.8 Zn, max. 0.005 Fe, 0.004 Cu, 0.003 Ni, 0.07 Si, max. 0.01 Cr, and balance Mg. The as-received AZ31 was in a cold rolled and partially annealed condition.

2.2. Coating Process

Sheet samples of 1 × 1 cm² were polished on both sides with SiC abrasive papers (up to 4000 grit) to obtain a uniform roughness. Samples were washed in acetone for 10 min in an ultrasonic bath to remove any surface contaminations. At the end of the surface preparation, samples were washed in deionized water and immediately dried in the air.

For the dip coating, dopamine hydrochloride ((HO)₂C₆H₃CH₂CH₂NH₂·HCl), hydrochloric acid (HCl), and tris(hydroxymethyl)aminomethane, also known as Tris, ((HOCH₂)₃CNH₂) were purchased from Merck (Darmstadt, Germany) as raw materials. The coating solution was prepared using 2 mg/mL dopamine hydrochloride, 100 mL deionized water, and 48 mM Tris as a buffer. In order to understand the oxidant effect on the coating, two different conditions were applied during the dip coating process: (1) the absence of oxygen in the solution and (2) the solution continuously being oxygenized with a flow rate of 0.4 L/min. In both conditions, the pH of the solution was adjusted to 8.5 and was kept constant by adding adequate amounts of hydrochloric acid with a concentration of 1 M. The pH value was monitored with a digital pH meter (Metrohm, Herisau, Switzerland).

The substrate was immersed in the solution for two hours in darkness [17,27]. After immersion, the samples were removed quickly to inhibit further oxidation and cleaned in deionized water to remove any unattached dopamine on the surface. Coated samples were finally dried in a nitrogen flow to avoid any undesirable surface oxidation. In this work, samples functionalized via dopamine with the absence of oxygen are designated as “dopa”, while samples immersed in a solution rich in oxygen are named “dopa-O”, and the pristine substrate is “AZ31”.

2.3. Characterization

The morphological feature observations, accompanied with a chemical analysis of the pristine and functionalized AZ31 alloys, were carried out using a field emission scanning electron microscope (FESEM, Mira3 Tescan, Brno, Czech Republic) equipped with an energy dispersive spectroscopy detector (EDS: EDAX- AMETEK, Tilburg, The Netherlands). FESEM images were taken in secondary electron mode to monitor the topography of the layer. Chemical analysis was carried at the surface and at the cross section to estimate the homogeneity of the deposited polydopamine. Moreover, Fourier transform infrared spectroscopy (FTIR, Thermo; Waltham, MA, USA) in transmittance mode was used to verify the presence of polymerized dopamine on the surface of the “dopa” and “dopa-O” samples.

2.4. Electrochemical Analysis

The degradation behavior of the samples was investigated via electrochemical impedance spectroscopy (EIS; AutoLab Potentiostat, Metrohm, Herisau, Switzerland). Samples were stabilized in phosphate-buffered saline (PBS) solution prior to the tests, and all impedance measurements were performed in a PBS solution at a temperature of 37 °C. A three-electrode electrochemical cell setup, with an Ag/AgCl electrode as a reference electrode and a platinum sheet as a counter electrode, was utilized in this work. Moreover, samples were used as working electrodes. EIS scans were acquired from 100 kHz to 0.01 Hz, and the impedance data were analyzed with the NOVA software (version 1.11).

2.5. Cell Cultivation

A human osteosarcoma cell line (G292), taken from National Cell Bank of Iran, was selected to evaluate the cellular behavior of samples. Osteoblast-like cells were cultured in a humidified atmosphere of 5% CO₂ at a temperature of 37 °C using Dulbecco’s modified Eagle’s medium (DMEM, BIO-IDEA, Iran) supplemented with 10% fetal bovine serum (FBS) (Gibco, Thermo, Waltham, MA, USA) and 1% antimicrobial penicillin/streptomycin solution 100X (Biosera, Kansas City, MO, USA). The cells were subcultured in a cell culture medium, which was refreshed every 3 days before utilization. Two series of samples were placed in 6-well plates and sterilized by ultraviolet light in 70% (V/V) ethanol–water solution and kept in sterilized media before analysis. Afterwards, samples were seeded with the same number of G292 cells (10⁵ cells) in a culture medium, and the cells were cultivated for 72 h in an incubator. Then, the samples were gently rinsed with phosphate-buffered saline solution (PBS) to remove the unattached cells.

Microscopic observations were carried out via both FESEM and fluorescent microscope to observe the cell morphology and adhesion to the samples. For the FESEM observation, the cells were fixed with a 2.5 v % glutaraldehyde solution for 2 h in a dark environment. Subsequently, the samples were gently washed again with PBS and then immersed in a bath of 50%, 60%, 70%, 80%, 90%, and 100% (V/V) ethanol / water solutions for 30 min each time to dehydrate the cells attached to their surfaces. The dehydration conducted in absolute ethanol was performed twice, and each time the samples were immersed in 100% ethanol for 1 h. The morphology of the G292 cells attached to the samples was observed after drying and sputtering with gold.

The cell behavior was also examined by a fluorescence microscope (Olympus, Japan) using a cell staining method. A total of 0.1% acridine orange (AO, sigma, Saint Louis, MO, USA) was utilized to visualize the remaining cells on the substrates [28], staining the cells for 1–2 min.

2.6. Molecular Dynamics Simulation

The effect of the oxidant on polydopamine coating was studied via molecular dynamics simulations. Two different conditions were designed, simulating the “dopa” (condition one) and “dopa-O” (condition 2) deposition conditions. In both conditions, the magnesium matrix was simulated via EAM (embedded atom model) potential. Moreover, each condition consisted of a mixture of dopamine monomers, indolequinone monomers, and dimmers. Concerning the oxidation mechanism of dopamine, the different ratios of dopamine to indolequinone were considered for each deposition condition: 90/10 for “dopa” and 10/90 for “dopa-O”. Molecular dynamics simulations were performed via a large-scale atomic/molecular massively parallel simulator (LAMMPS). The atomic computations were carried out in periodic boundaries and in three dimensions. The generic force field, Dreiding, was employed to describe the inter-molecular interactions of the polymer. In this case, the valence interactions were considered to be bond stretch, bond-angle bend, and dihedral angle torsion terms [29]. The non-bonded or Van der Waals interactions of polymer/polymer and polymer/Mg are given by the Lennard–Jones [30] potential. A total of 10,000,000 time-steps with an increment of 0.01 fs were simulated for each condition. The temperatures of the conditions were controlled using a Langevin thermostat accompanied by a micro-canonical ensemble NVE. Visualizations were created using the Ovito software.

3. Results

3.1. Characterization of the Coating

The surface observation and the elemental map analysis of “AZ31”, “dopa”, and “dopa-O” conditions are displayed in Figure 1. In the as-received “AZ31” condition, intermetallic phases rich in aluminum are observed on the polished surface, which is reported as a typical secondary phase $Mg_{17}Al_{12}$ in AZ31 alloy [31,32]. Figure 1b, c shows the functionalized surface of the “dopa” and “dopa-O”. Both samples are homogeneously covered with a coating, which exhibits the presence of nitrogen and oxygen on the Mg matrix, in concordance with observations in the literature, together with carbon and hydrogen elements in the polydopamine layer [24]. At the surface of the coating, cracks are formed during the drying stage [33].

A cross section of the coated samples is analyzed in Figure 2 to determine the thickness of the layer, and the variation of the elements depends on the dip condition. The thickness of the coatings was 42 and 85 μm for “dopa” and “dopa-O”, respectively, in agreement with both SEM observations and element profile scans. The element scan line shows a strong influence of the type of coating on the amount of nitrogen and oxygen elements in the layers. The “dopa-O” has higher intensity than the “dopa” condition. Furthermore, the presence of Mg in the layer of “dopa-O” may be related to the oxidation of the substrate due to the flow of oxygen during the coating process. The element profile in Figure 2c shows that although the amount of element is lower in “dopa”, it is more homogenous in composition than that the “dopa-O”. The first 20 μm (Region I) keeps a constant composition for both conditions, while the reduction of N through the coating in “dopa-O” (region II) indicates a lack of polydopamine in this area, which has been replaced by magnesium oxide.

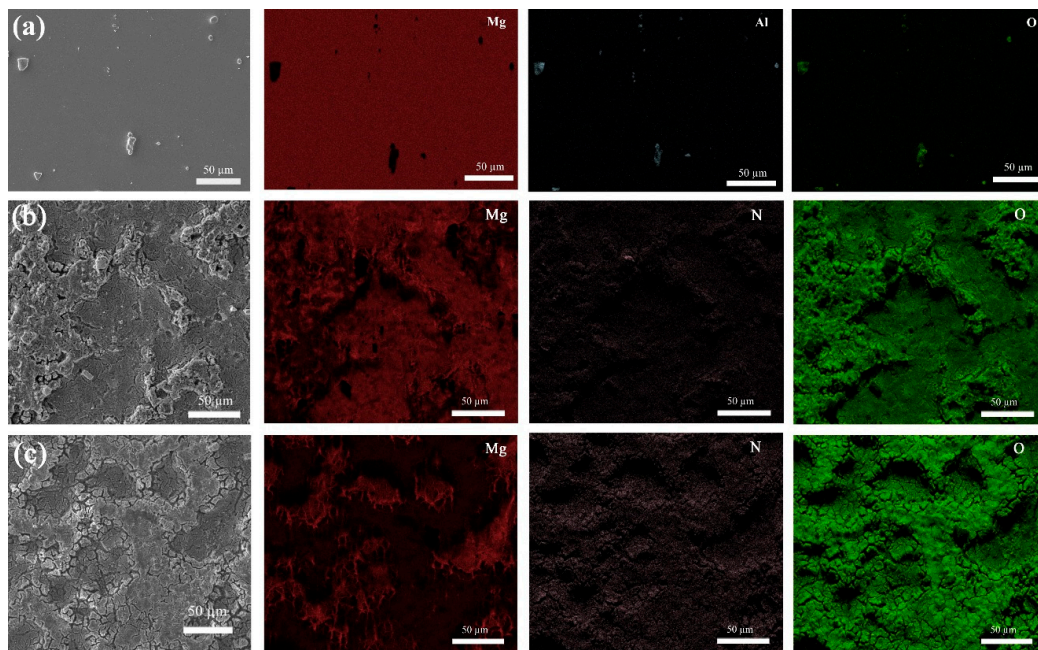


Figure 1. The SEM micrographs and relative elemental mapping of (a) the as-received AZ31 alloy; (b) “dopa” and (c) “dopa-O”. Samples functionalized via dopamine with the absence of oxygen are designated as “dopa”, while samples immersed in a solution rich in oxygen are named “dopa-O”.

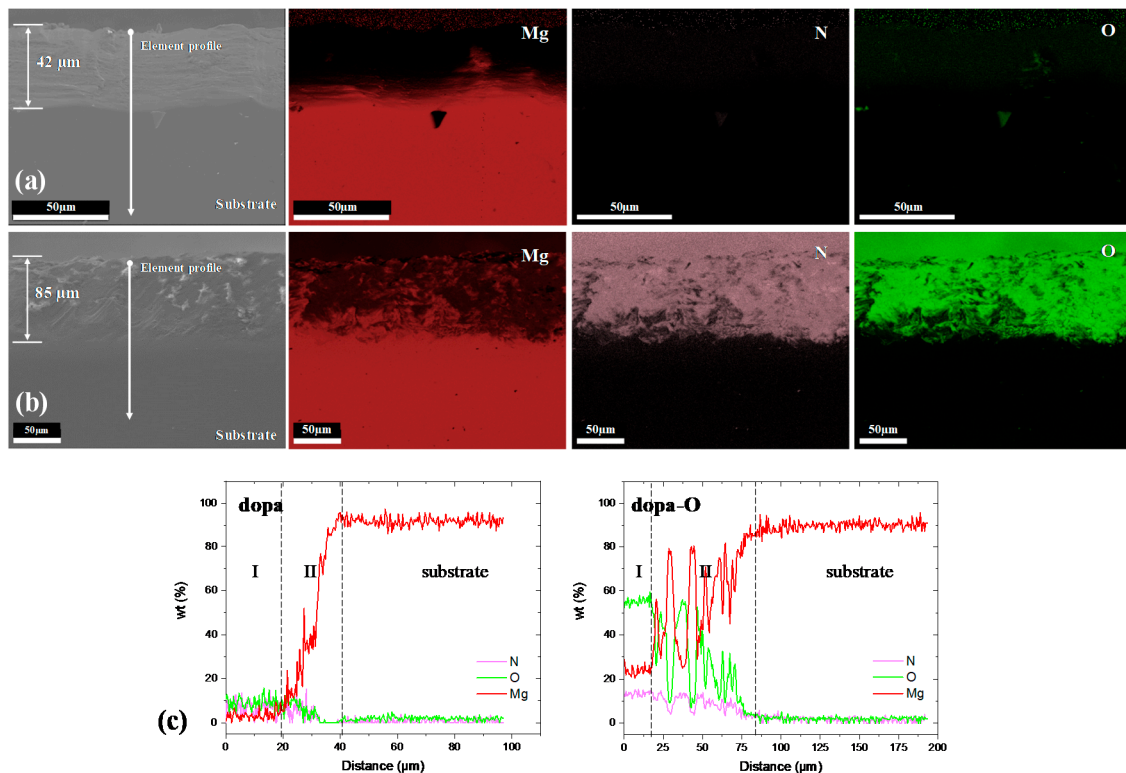


Figure 2. SEM micrographs and relative elemental mapping of the cross section (a) “dopa” and (b) “dopa-O”; (c) elemental line scan of “dopa” and “dopa-O” coatings, marked in the micrographs in (a) and (b), respectively.

FTIR characterizations detect the functional groups in the polydopamine layer. The functional groups of the formed polymeric layer on the surface of “dopa” and “dopa-O” are depicted in Figure 3. A peak at 702 cm^{-1} can be observed in the “dopa” curve, which implies the ring deformation vibration

of 1,2,4-trisubstituted benzene. In both conditions, the peaks at 800 cm^{-1} (and also the band broadening between 800 and 860 cm^{-1}) can be attributed to the C–H wagging vibration of the ring hydrogens in the 1,2,4-trisubstituted and 1,2,4,5-tetrasubstituted benzenes. The band accompanied with peaks in the range of 950 – 1420 cm^{-1} is ascribed to ring deformation vibrations and C–N stretching vibrations [34]. The adsorption bands located in the range of 1450 – 1625 cm^{-1} originate from the C=C stretching vibration of benzene rings and the N–H bending [27]. In addition, a peak at 1637 for both conditions is attributed to the C=C stretching vibrations, while the “dopa-O” condition shows a peak at 1729 cm^{-1} related to the C=O stretching vibrations [34]. A broad absorbance in the spectrum between 3100 and 3600 cm^{-1} is ascribed to N–H/O–H stretching vibrations [33], and in this region, NH and NH_2 stretching vibrations happen in the range of 3100 – 3360 cm^{-1} [34].

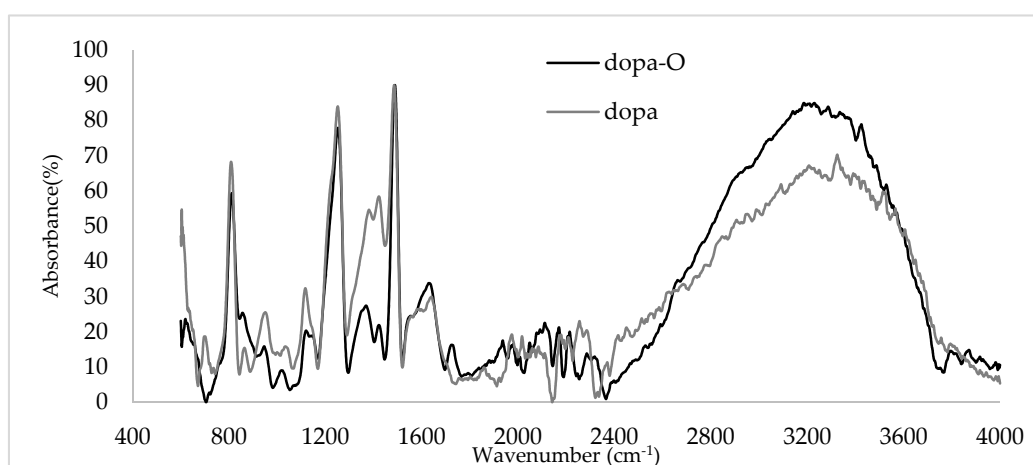


Figure 3. The Fourier transform infrared spectroscopy (FTIR) spectrum of “dopa” and “dopa-O”.

3.2. Electrochemical Properties

The effect of oxygen on the corrosion resistance of the coated samples was analyzed by impedance tests in a PBS solution at $37\text{ }^{\circ}\text{C}$. The variation of the real impedance component (Z') versus the imaginary impedance component (Z''), the Nyquist plot, is shown in Figure 4a. The Bode plots (given in Figure 4c,d) improve the accuracy of the degradation behavior. Herein, the consistency of the obtained EIS data are evaluated with the Kramers–Kronig (K–K) transformation. The impedance spectra of all samples are characterized in high and medium frequency regions, with one semicircle loop in the Nyquist plot. Moreover, the one phase extremum in the Bode plot (Figure 4c) is an indicator of one semicircle in the Nyquist plot (Figure 4a). Figure 4d illustrates the decrease in impedance when the frequency decreases. This process is influenced by the adsorbed intermediate species, which form layers of corrosion products [35].

To compare the impedance data of the samples in quantity, the impedance plots are fitted with an equivalent electrical circuit, which is depicted in Figure 4b. The semicircle in the high and medium frequency region is ascribed as the constant phase element (CPE), simulating the charge transfer resistance (R_c) in parallel with the electric double layer. Moreover, the inductive loop is simulated by the inductance (L) and the relative inductive resistance (R_l). The total circuit is in series with the solution resistance (R_s).

The impedance data extracted from the equivalent electrical circuit are given in Table 1. From the data, the quantity of the circuit elements is increased in the following order: “dopa-O” > AZ31 > “dopa”. Due to the insufficient quality of the polymer coating, the impedance is decreased in the “dopa”. However, the “dopa-O” sample shows the highest constant phase element, inductance, and real resistances. Apparently, the presence of oxygen gas flowing during the dopamine dip coating process improves the corrosion resistance of the functionalized AZ31 alloy.

Table 1. The extracted impedance data from equivalent electrical circuit. CPE, constant phase element.

Sample	R_s ($\Omega \text{ cm}^2$)	R ($\Omega \text{ cm}^2$)	CPE ($\mu\text{Mho}/\text{cm}^2$)	N	R_l ($\Omega \text{ cm}^2$)	L (H cm^2)	X^2 (<0.5)
AZ31	22.1	68.7	39.6	0.841	38.3	13.9	0.385
dopa	13.152	31.44	50.83	0.652	15.408	71.52	0.427
dopa-O	15.38	142.32	105.83	0.718	185.52	264	0.206

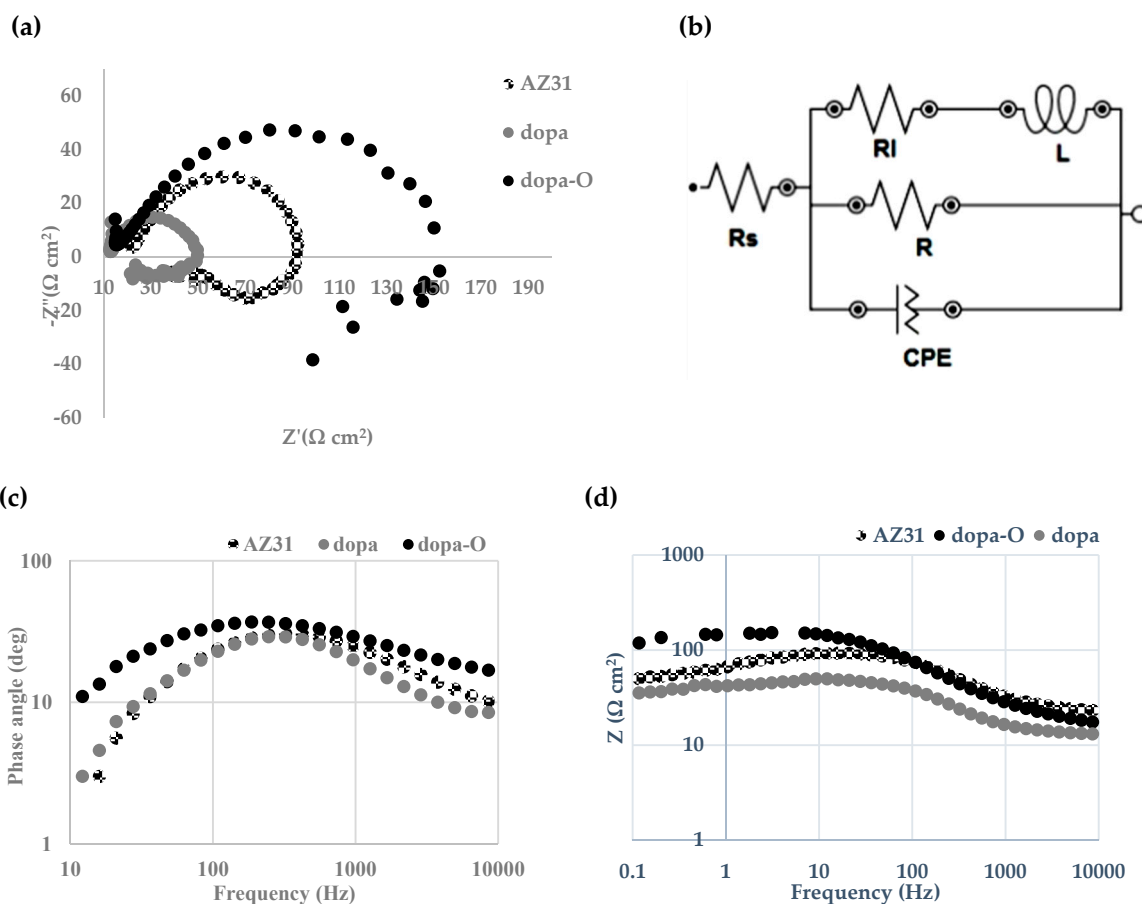


Figure 4. Electrochemical data for samples; “AZ31”, “dopa”, and “dopa-O” (a) Nyquist plot; (b) Equivalent electrical circuit; (c) Bode-phase angle plot, and (d) Bode-impedance plot.

3.3. Cell Cultivation

The SEM micrographs of the G292 cells attached to the samples, after 72 h cultivation, are illustrated in Figure 5. Artifacts observed on the surface might be related to the sputtering with gold. The cells keep a rounded and spherical shape and show a slightly tendency to be spread out on the surface of the “AZ31” alloy and “dopa” (Figure 5a,b). However, the cells also show a tendency to spread out on the surface of the “dopa-O” condition, as illustrated in Figure 5c.

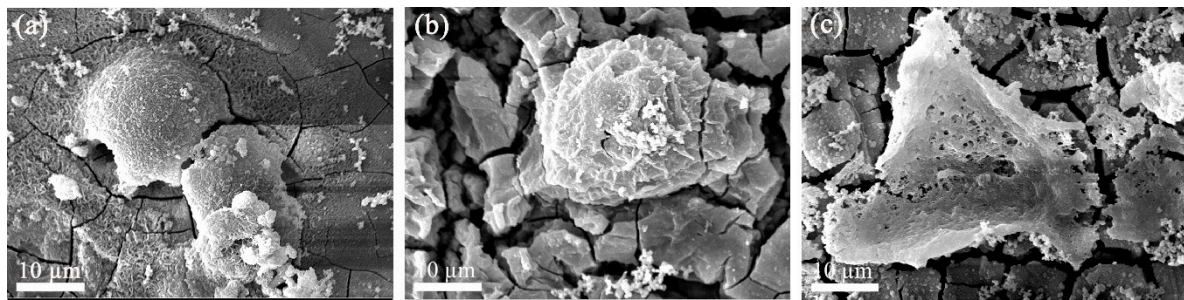


Figure 5. SEM micrographs of the adherent G292 cells, (a) “AZ31”; (b) “dopa”; and (c) “dopa-O” after 72 h of cultivation time.

Figure 6 shows the G292 cells attached on the surface of samples by fluorescent microscopy. The adhesion of the cells can be evidenced in all the cases and a change of the cell’s behavior in the “dopa-O” condition is perceptible. However, this information is not enough to draw the effect of the coating on the cell’s morphology due to the cytoskeleton/membrane cannot be observed properly. Further investigations focused on cell viability and proliferation are needed to better quantify the effect of the oxygen on the cells’ behavior.

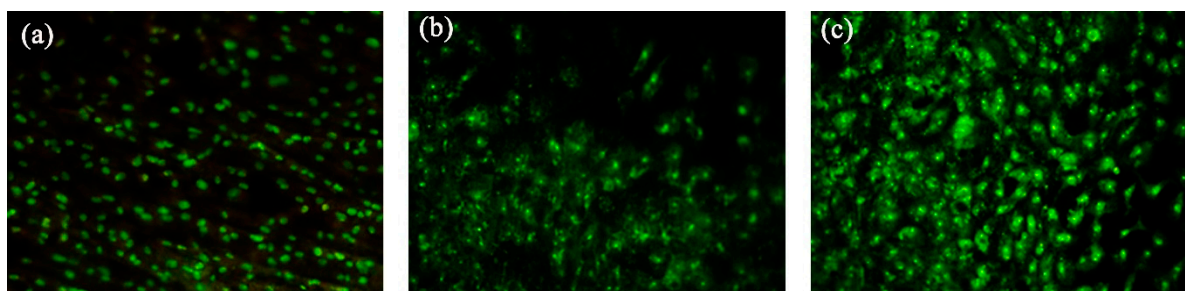


Figure 6. Fluorescent microscopy of adherent cells stained with acridine orange: (a) “AZ31”; (b) “dopa”; and (c) “dopa-O” after 24 h of cultivation time; (Magnification 100×).

3.4. Molecular Dynamics Simulation

Molecular dynamics simulations help to determine the effect of oxidants on the polydopamine of the AZ31 alloy substrate. The displacement of the polymer mass towards the substrate surface was simulated. Thus, the center-of-mass (com) command was computed in LAMMPS for Z direction. Additionally, two different conditions were implemented by LAMMPS, considering that the dopamine molecule transforms into indolequinone in the presence of oxygen [25], as described in Section 2.6. The dimmers were designed for both conditions due to the further interactions between the monomer molecules [36]. In fact, polydopamine is not a covalent bond polymer but instead an aggregate of monomers held together by noncovalent forces [24]. The designed molecular structures of dopamine and indolequinone monomers [25], along with the dimmers [24], are illustrated in Figure 7a–c. In addition, the visualized conditions (one and two) are illustrated in Figure 7d,e. The displacements of the center-of-mass (com) in the polymer were calculated for each time-step in the Z direction, shown in Figure 7f. The slope of the graphs represents the difference of the displacement per difference of time. Hence, the slope indicates the deposition rate (angstrom/femtosecond). In this work, the slope of the “dopa-O” condition is higher, showing that the presence of oxygen accelerates the deposition of the polymer on the substrate. It seems that the tendency of indolequinone to bond to the substrate is higher than that of dopamine during the coating process.

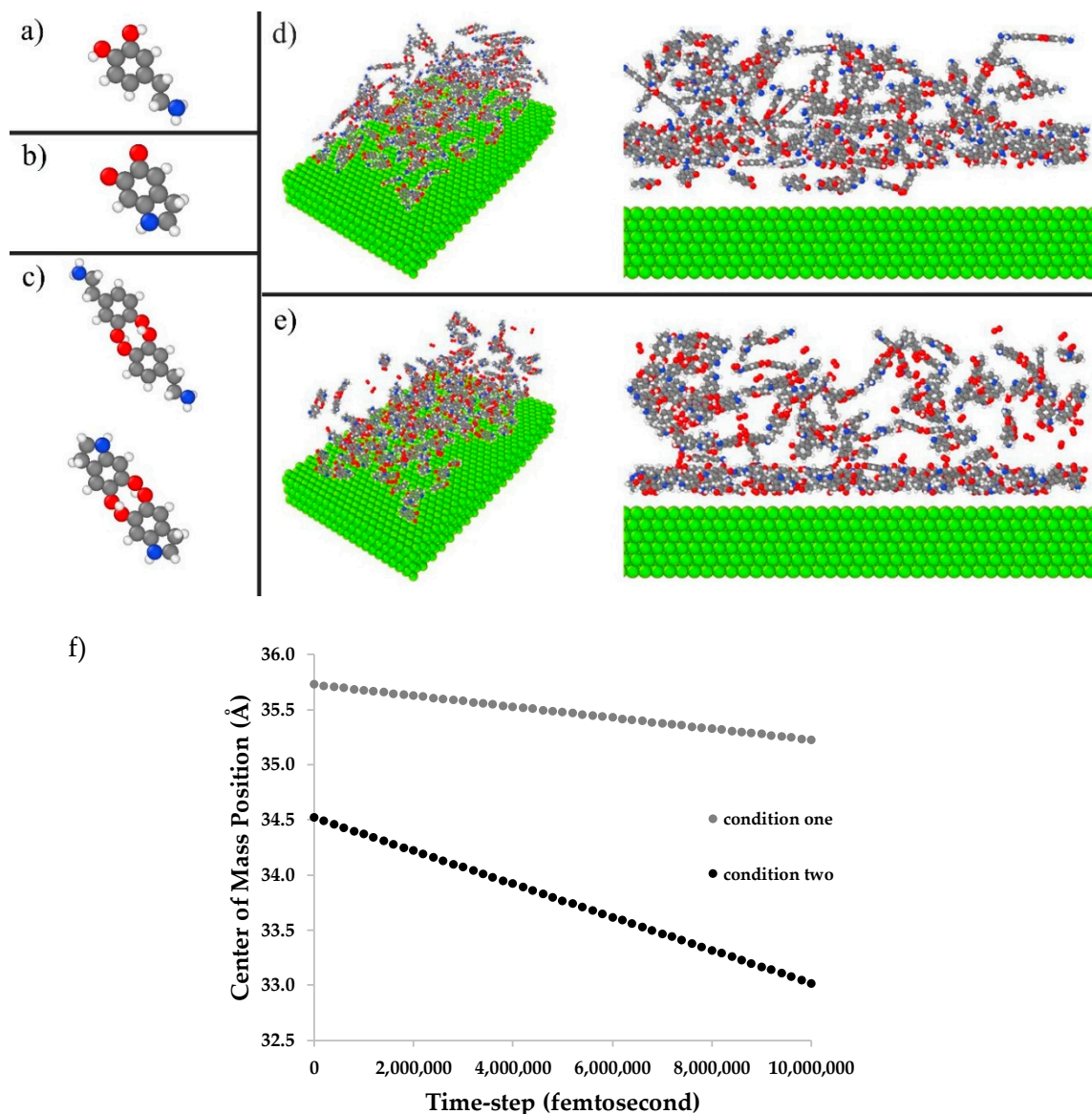


Figure 7. Molecular dynamic simulation: (a) Dopamine monomer and (b) indolequinone monomer; (c) dimers; (d) condition one; (e) condition two; (colors definition: green: Mg; gray: C; white: H; red: O and blue: N); (f) center of mass versus time-step.

4. Discussion

4.1. Characterization of the Coating

The oxidant can intensify polydopamine formation [18,25]. According to the EDS maps given in Figure 1, the surface of the “dopa” and “dopa-O” is covered homogeneously with oxygen and nitrogen. The thickness measurements given in Figure 2 indicate that the thickness of the coating layer in “dopa-O” is, relatively, twice that of “dopa”, in agreement with the deposition rate estimated by molecular dynamic simulations (Figure 7f). From respective cross section EDS mapping, the difference in nitrogen and oxygen content is obvious. This difference can be further perceived from the element profile scans (Figure 2c). The coatings (in depth) show two main regions, where the depth of region I is relatively the same for both conditions (~20 μm). Region II shows more depth for the “dopa-O”, and the presence of Mg in both layers might be related to the magnesium oxide formed during the immersion in the dip process. This effect is more noticeable in the “dopa-O” condition, where the

continuous flowing of gas can promote the formation and growth of the oxide at the surface. On the other hand, a difference between the two conditions with respect to the ratio of oxygen to nitrogen in weight percent (O/N) is pronounced. Region I indicates a ratio of around 3 for “dopa-O” and 1 for “dopa”. The presence of polydopamine should show a ratio of O/N in dopamine and an indolequinone ratio of 2. For this reason, the presence of these molecules on the surface of “dopa” is more reliable in this work. Analysis of the polydopamine layer via FTIR spectrum (Figure 3) indicated that the NH and NH₂ stretching vibrations take place in the wavenumber range, 3100–3360 cm⁻¹ [34], and a higher absorbance of “dopa-O” is associated with the amount of nitrogen (Figure 2c). Through the oxidation mechanism of polydopamine, the dopamine molecules transform to indolequinone molecules, whose structure is benzene-like with different positions for the substitutes. Here, the three-substituted structure of dopamine changes to the four-substituted structure of indolequinone [25]. The peak at 702 cm⁻¹ in “dopa” is due to the ring deformation vibration of 1,2,4-trisubstituted benzene, which is similar to the dopamine structure [34]. Thus, a high amount of dopamine that is not fully oxidized can still be expected in the coating of the “dopa”. If oxidation and cyclization do not take place completely, dopamine molecules co-exist in the solution [37].

On the other hand, the peak at 800 cm⁻¹ and the band broadening between 800 and 860 cm⁻¹ are attributed to the C–H wagging vibration of ring hydrogens in 1,2,4-trisubstituted and 1,2,4,5-tetrasubstituted benzenes [34]. This peak and band are slightly higher in the “dopa-O” condition, which has a similar structure to 1,2,4,5-tetrasubstituted benzenes. This means that the presence of oxygen activates the oxidation mechanism, and more three-substituted benzenes (dopamine structures) transform into four-substituted benzenes (indolequinone structures). Moreover, the appearance of a peak at 1729 cm⁻¹ for “dopa-O” is due to the carbonyl (C=O) stretching vibrations of the indolequinone [24,25,34] structure, showing that adding oxygen increases the ratio of the dopamine that transforms to indolequinone. This effect promotes the presence of polydopamine instead of dopamine molecules in the “dopa-O” condition.

4.2. Electrochemical Properties

A comparison of the impedance responses to the corrosive PBS solution (Figure 4a) shows that the largest semicircle is in the “dopa-O” condition, thereby validating the observations of Kim et al. in various commercial microporous membranes [38]. The amount of the constant phase element, representing the resistance to the adsorption/diffusion processes at the electrode surface [39], increased from 50.83 μMho/cm² in “dopa” to 105.83 μMho/cm² in “dopa-O”. Thus, the impedance of the capacity behavior (CPE) is relatively doubled (see Table 1). This trend is also observed for real resistors. The charge transfer resistance increased from 31.44 Ω cm² in “dopa” to 142.32 Ω cm² in “dopa-O”. Thus, the transferring of charges responsible for anodic and cathodic reactions is hindered in “dopa-O”, so the formed polymeric layer on “dopa-O” acts as a stronger inhibitor of charge transfer and charge storage (CPE) than “dopa”. Moreover, there is a considerable increase in inductance element values after surface functionalization in the presence of oxygen, representing greater prevention against species movement, including Mg²⁺ and Mg(OH)₂. On the other hand, the equivalent circuit component values of “dopa” are lower than those of “AZ31”. It seems that the polymeric layer formed on the surface of “dopa” cannot act as an effective barrier to magnesium dissolution in the corrosive PBS solution.

The polymeric layer formed in the “dopa-O” deposition condition acts as a superior barrier layer to PBS corrosive media. As seen in the EDS line (Figure 2c), region I in “dopa-O” contains a higher O/N ratio. Further, according to the FTIR view, the functional layer groups indicate a greater oxidation state. Since oxidation is the polymerization mechanism, it can be deduced that the polymerization of dopamine takes place more frequently on “dopa-O”. Through dopamine polymerization or polydopamine formation, aggregates are formed on the surface by linking the particles together [33]. Therefore, this layer can act as a better barrier than “dopa” against corrosive liquid penetration, with less oxidized dopamine in the layer. On the other hand, the presence of MgO in “dopa-O” might influence the corrosion resistance of the material.

5. Conclusions

The use of oxygen as an oxidant agent for the dopamine functionalizing process was considered in this work, using the magnesium alloy AZ31. The introduction of oxygen into the dip coating draws the following conclusions:

- The molecular dynamic simulation and FTIR analysis show an improvement in the deposition rate and the presence of polydopamine on the substrate.
- The addition of oxygen increases the impedance response of the AZ31 alloy.
- The formation of polydopamine with the presence of amino and hydroxyl functional groups on the surface of the material might be promising for the cell's response. Further investigations focused on the cell viability and proliferation are necessary to confirm the biocompatibility of the coating.

Author Contributions: Conceptualization, F.W., A.G. and A.Z.; methodology, A.Z.; software, A.G.; formal analysis, A.G. and F.W.; investigation, F.W. and A.G.; writing—original draft preparation, A.G., F.W. and A.Z.; writing—review and editing, A.G., F.W., C.S. and A.Z.; supervision, A.Z. and C.S.

Funding: This research received no external funding.

Acknowledgments: Open Access Funding by the Graz University of Technology. Authors would like to thank R. Buzolin for FESEM observations, A. Bordbar-Khiabani for samples preparation, T. Ramezani for helping with cell cultivation and R. Sabetvand for supporting the molecular dynamics simulations.

Conflicts of Interest: The authors declare no conflict of interest.

References

1. Witte, F.; Hort, N.; Vogt, C.; Cohen, S.; Kainer, K.U.; Willumeit, R.; Feyerabend, F. Degradable biomaterials based on magnesium corrosion. *Curr. Opin. Solid State Mater. Sci.* **2008**, *12*, 63–72. [[CrossRef](#)]
2. Gu, X.N.; Zheng, Y.F. A review on magnesium alloys as biodegradable materials. *Front. Mater. Sci. Chin.* **2010**, *4*, 111–115. [[CrossRef](#)]
3. Ghaffarpasand, F.; Shahrezaei, M.; Dehghankhalili, M. Effects of platelet rich plasma on healing rate of long bone non-union fractures: A randomized double-blind placebo controlled clinical trial. *Bull. Emerg. Trauma* **2016**, *4*, 134–140. [[PubMed](#)]
4. Shahrezaei, M.; Salehi, M.; Keshtkari, S.; Oryan, A.; Kamali, A.; Shekarchi, B. In vitro and in vivo investigation of pla/pcl scaffold coated with metformin-loaded gelatin nanocarriers in regeneration of critical-sized bone defects. *Nanomedicine* **2018**, *14*, 2061–2073. [[CrossRef](#)] [[PubMed](#)]
5. Wagener, V.; Schilling, A.; Mainka, A.; Hennig, D.; Gerum, R.; Kelch, M.-L.; Keim, S.; Fabry, B.; Virtanen, S. Cell adhesion on surface-functionalized magnesium. *ACS Appl. Mater. Interfaces* **2016**, *8*, 11998–12006. [[CrossRef](#)] [[PubMed](#)]
6. Wagener, V.; Killian, M.S.; Turhan, C.M.; Virtanen, S. Albumin coating on magnesium via linker molecules—comparing different coating mechanisms. *Colloids Surf. B Biointerfaces* **2013**, *103*, 586–594. [[CrossRef](#)] [[PubMed](#)]
7. Cui, W.; Beniash, E.; Gawalt, E.; Xu, Z.; Sfeir, C. Biomimetic coating of magnesium alloy for enhanced corrosion resistance and calcium phosphate deposition. *Acta Biomater.* **2013**, *9*, 8650–8659. [[CrossRef](#)] [[PubMed](#)]
8. Zhu, B.; Xu, Y.; Sun, J.; Yang, L.; Guo, C.; Liang, J.; Cao, B. Preparation and characterization of aminated hydroxyethyl cellulose-induced biomimetic hydroxyapatite coatings on the AZ31 magnesium alloy. *Metals* **2017**, *7*, 214. [[CrossRef](#)]
9. Tiyyagura, H.R.; Fuchs-Godec, R.; Gorgieva, S.; Arthanari, S.; Mohan, M.K.; Kokol, V. Biomimetic gelatine coating for less-corrosive and surface bioactive Mg–9Al–1Zn alloys. *J. Mater. Res.* **2018**, *33*, 1449–1462. [[CrossRef](#)]
10. Lee, H.; Rho, J.; Messersmith, P.B. Facile conjugation of biomolecules onto surfaces via mussel adhesive protein inspired coatings. *Adv. Mater.* **2009**, *21*, 431–434. [[CrossRef](#)] [[PubMed](#)]

11. Yang, X.; Zhu, L.; Tada, S.; Zhou, D.; Kitajima, T.; Isoshima, T.; Yoshida, Y.; Nakamura, M.; Yan, W.; Ito, Y. Mussel-inspired human gelatin nanocoating for creating biologically adhesive surfaces. *Int. J. Nanomed.* **2014**, *9*, 2753–2765.
12. Zhou, X.; Ouyang, J.; Li, L.; Liu, Q.; Liu, C.; Tang, M.; Deng, Y.; Lei, T. In vitro and in vivo anti-corrosion properties and biocompatibility of 5 β -TCP/Mg-3Zn scaffold coated with dopamine-gelatin composite. *Surf. Coat. Technol.* **2019**, *374*, 152–163. [[CrossRef](#)]
13. Xu, C.; Xu, K.; Gu, H.; Zheng, R.; Liu, H.; Zhang, X.; Guo, Z.; Xu, B. Dopamine as a robust anchor to immobilize functional molecules on the iron oxide shell of magnetic nanoparticles. *J. Am. Chem. Soc.* **2004**, *126*, 9938–9939. [[CrossRef](#)] [[PubMed](#)]
14. Liu, Y.; Xu, C.; Gu, Y.; Shen, X.; Zhang, Y.; Lie, B.; Chen, L. Polydopamine-modified poly(l-lactic acid) nanofiber scaffolds immobilized with an osteogenic growth peptide for bone tissue regeneration. *R. Soc. Chem. Rsc Adv.* **2019**, *9*, 11722–11736. [[CrossRef](#)]
15. Huang, L.; Yi, J.; Gao, Q.; Wang, X.; Chen, Y.; Liu, P. Carboxymethyl chitosan functionalization of cped-treated magnesium alloy via polydopamine as intermediate layer. *Surf. Coat. Technol.* **2014**, *258*, 664–671. [[CrossRef](#)]
16. Singer, F.; Schlesak, M.; Mebert, C.; Höhn, S.; Virtanen, S. Corrosion properties of polydopamine coatings formed in one-step immersion process on magnesium. *Appl. Mater. Interfaces* **2015**, *7*, 26758–26766. [[CrossRef](#)]
17. Lin, B.; Zhong, M.; Zheng, C.; Cao, L.; Wang, D.; Wang, L.; Liang, J.; Cao, B. Preparation and characterization of dopamine-induced biomimetic hydroxyapatite coatings on the AZ31 magnesium alloy. *Surf. Coat. Technol.* **2015**, *281*, 82–88. [[CrossRef](#)]
18. Lyngø, M.E.; Westen, R.V.D.; Postma, A.; Stadler, B. Polydopamine—A nature-inspired polymer coating for biomedical science. *Nanoscale* **2011**, *3*, 4916–4928. [[CrossRef](#)]
19. Lee, H.; Dellatore, S.M.; Miller, W.M.; Messersmith, P.B. Mussel-inspired surface chemistry for multifunctional coatings. *Science* **2007**, *318*, 426–430. [[CrossRef](#)]
20. Yang, H.-C.; Wu, Q.-Y.; Wan, L.-S.; Xu, Z.-K. Polydopamine gradients by oxygen diffusion controlled autoxidation. *Chem. Commun.* **2013**, *49*, 10522–10524. [[CrossRef](#)]
21. Sedó, J.; Saiz-Poseu, J.; Busqué, F.; Ruiz-Molina, D. Catechol-based biomimetic functional materials. *Adv. Mater.* **2013**, *25*, 653–701. [[CrossRef](#)] [[PubMed](#)]
22. Hu, H.; Dyke, J.C.; Bowman, B.A.; Ko, C.-C.; You, W. Investigation of dopamine analogues: Synthesis, mechanistic understanding and structure-property relationship. *Langmuir* **2016**, *32*, 9873–9882. [[CrossRef](#)] [[PubMed](#)]
23. Herlinger, E.; Jameson, R.F.; Linert, W. Spontaneous autoxidation of dopamine. *J. Chem. Soc. Perkin Trans.* **1995**, *2*, 259–263. [[CrossRef](#)]
24. Dreyer, D.R.; Miller, D.J.; Freeman, B.D.; Paul, D.R.; Bielawski, C.W. Elucidating the structure of poly(dopamine). *Langmuir* **2012**, *28*, 6428–6435. [[CrossRef](#)] [[PubMed](#)]
25. Bernsmann, F.; Ball, V.; Addiego, F.; Ponche, A.; Michel, M.; Gracio, J.J.D.A.; Toniazzi, V.; Ruch, D. Dopamine-melanin film deposition depends on the used oxidant and buffer solution. *Langmuir* **2011**, *27*, 2819–2825. [[CrossRef](#)] [[PubMed](#)]
26. Ponzio, F.; Barthes, J.; Bour, J.; Michel, M.; Bertani, P.; Hemmerle, J.; d’Ischia, M.; Ball, V. Oxidant control of polydopamine surface chemistry in acids: A mechanism-based entry to superhydrophilic-superoleophobic coatings. *Chem. Mater.* **2016**, *28*, 4697–4705. [[CrossRef](#)]
27. Zhang, L.; Mohammed, E.A.A.; Adriaens, A. Synthesis and electrochemical behavior of a magnesium fluoride-polydopamine-stearic acid composite coating on AZ31 magnesium alloy. *Surf. Coat. Technol.* **2016**, *307*, 56–64. [[CrossRef](#)]
28. Szaraniec, B.; Pielichowski, K.; Pac, E.; Menaszek, E. Multifunctional polymer coatings for titanium implants. *Mater. Sci. Eng. C* **2018**, *93*, 950–957. [[CrossRef](#)] [[PubMed](#)]
29. Mayo, S.L.; Olafson, B.D.; Goddard, W.A. Dreiding: A generic force field for molecular simulations. *J. Phys. Chem.* **1990**, *94*, 8897–8909. [[CrossRef](#)]
30. Panteva, M.T.; Giambasu, G.M.; York, D.M. Force field for Mg²⁺, Mn²⁺, Zn²⁺, and Cd²⁺ ions that have balanced interactions with nucleic acids. *J. Phys. Chem.* **2015**, *119*, 15460–15470. [[CrossRef](#)] [[PubMed](#)]
31. Kim, H.S.; Kim, G.H.; Kim, H.; Kim, W.J. Enhanced corrosion resistance of high strength Mg–3Al–1Zn alloy sheets with ultrafine grains in a phosphate-buffered saline solution. *Corros. Sci.* **2013**, *74*, 139–148. [[CrossRef](#)]
32. Pawar, S.; Zhou, X.; Thompson, G.E.; Scamans, G.; Fan, Z. The role of intermetallics on the corrosion initiation of twin roll cast AZ31 mg alloy. *J. Electrochem. Soc.* **2015**, *162*, C442–C448. [[CrossRef](#)]

33. Jiang, J.; Zhu, L.; Zhu, L.; Zhu, B.; Xu, Y. Surface characteristics of a self-polymerized dopamine coating deposited on hydrophobic polymer films. *Langmuir* **2011**, *27*, 14180–14187. [[CrossRef](#)] [[PubMed](#)]
34. Simons, W.W. *The Sadtler Handbook of Infrared Spectra*; Sadtler Research Laboratories: Philadelphia, PA, USA, 1978.
35. Orazem, M.E.; Orazem, M. *Electrochemical Impedance Spectroscopy*; John Wiley & Sons: Hoboken, NJ, USA, 2008.
36. Orishchin, N.; Crane, C.C.; Brownell, M.; Wang, T.; Jenkins, S.; Min Zou, A.N.C. Rapid deposition of uniform polydopamine coatings on nanoparticle surfaces with controllable thickness. *Langmuir* **2017**, *33*, 6046–6053. [[CrossRef](#)] [[PubMed](#)]
37. Ding, Y.H.; Floren, M.; Tan, W. Mussel-inspired polydopamine for bio-surface functionalization. *Biosurface Biotribol.* **2016**, *2*, 121–136. [[CrossRef](#)]
38. Kim, H.W.; McCloskey, B.D.; Choi, T.H.; Lee, C.; Kim, M.J.; Freeman, B.D.; Park, H.B. Oxygen concentration control of dopamine-induced high uniformity surface coating chemistry. *ACS Appl. Mater. Interfaces* **2013**, *5*, 223–238.
39. Lasia, A. *Electrochemical Impedance Spectroscopy and Its Applications*; Springer: New York, NY, USA, 2014.



© 2019 by the authors. Licensee MDPI, Basel, Switzerland. This article is an open access article distributed under the terms and conditions of the Creative Commons Attribution (CC BY) license (<http://creativecommons.org/licenses/by/4.0/>).